Physics Criteria for a Subscale Plasma Liner Experiment

Hsu, Scott C.
Thio, Yong C. Francis

Physics Criteria for a Subscale Plasma Liner Experiment

Scott C. Hsu · Y. C. Francis Thio

Abstract Spherically imploding plasma liners, formed by merging hypersonic plasma jets, are a proposed stand-off driver to compress magnetized target plasmas to fusion conditions [S. C. Hsu et al., IEEE Trans. Plasma Sci. **40**, 1287 (2012)]. In this paper, the parameter space and physics criteria are identified for a subscale, plasma-liner-formation experiment to provide data, e.g., on liner ram-pressure scaling and uniformity, that are relevant for addressing scientific issues of full-scale plasma liners required to achieve fusion conditions. Based on these criteria, we quantitatively estimate the minimum liner kinetic energy and mass needed, which informed the design of a subscale plasma liner experiment now under development.

1 Introduction

Ongoing research [1] on the Plasma Liner Experiment (PLX) [2,3] is aiming to demonstrate the formation and implosion of spherical plasma liners via merging hypersonic plasma jets formed by pulsed coaxial guns (where "hypersonic" refers to the jets being highly supersonic and where atomic excitation, ionization, and

Scott C. Hsu
Los Alamos National Laboratory, Los Alamos, NM 87545
Tel.: +1-505-667-3386
E-mail: scotthsu@lanl.gov

Y. C. Francis Thio
HyperJet Fusion Corporation, Chantilly, VA 20151
Tel: +1-301-524-4698
E-mail: francis.thio@hyperjetfusion.com

radiative effects are important [4]). The guns, jets, and imploding plasma liner constitute a *driver* to compress a magnetized plasma *target* to fusion conditions, i.e., a proposed embodiment of magneto-inertial fusion (MIF) [5,6,7] known as plasma-jet-driven magneto-inertial fusion (PJMIF) [8,9,10,11]. PJMIF has several attributes making it a potential candidate for an economically viable, repetitively pulsed fusion reactor [12]. An immediate, near-term objective is to retire the major physics risks associated with the plasma-liner-driver aspects of PJMIF at the lowest-possible cost and technical risk.

The key goal of PJMIF development during the present three-year research phase (ending in 2019) is to demonstrate the formation, viability, and scalability of spherically imploding plasma liners formed by merging plasma jets. Specifically, an objective is to obtain experimental data on two key scientific issues of the plasma liner as an MIF compression driver: (1) scaling of peak ram pressure (ρv^2) of the plasma liner versus initial plasma jet parameters and number of jets, and (2) evolution and control of non-uniformities seeded by the jet-merging process, which have the potential to degrade the ability of a plasma liner to compress a target plasma to fusion conditions.

Because the overall cost of a plasma-liner-formation experiment is closely linked to the initial stored energy, we were motivated to conduct a careful analysis of the minimum stored energy required to address PJMIF-relevant, plasma-liner issues in a meaningful way. The required stored energy is determined by two independent properties: (1) the electrical efficiency of the plasma guns, and (2) the required minimum initial kinetic energy of the imploding plasma liner. This paper is restricted to consideration of the latter. The analysis is based on first identifying key physics criteria that must be satisfied in order for a subscale experiment to pro-

vide data that is relevant for a full-scale, fusion-relevant plasma liner. Based on these criteria, we then quantitatively estimate the minimum initial plasma-liner kinetic energy and mass of a subscale experiment that satisfies the fusion-relevant plasma-liner criteria.

A full-scale PJMIF plasma liner [8,10] would consist of an array of, perhaps, hundreds of coaxial plasma guns uniformly mounted around a spherical chamber that is several meters in radius. It is envisioned [10] that a small subset of the guns fires first to form a magnetized plasma target, followed immediately by the remainder of the guns firing to form a spherically imploding plasma liner that compresses the target. The physical processes and steps of plasma-liner formation via merging plasma jets, the subsequent convergence of the liner, and scalings of peak liner ram pressure and non-uniformity evolution have been studied extensively and presented elsewhere [8,9,13,14,15,10,16,2, 17,18,19,20,21,22,23], though much more research is needed to validate the PJMIF concept.

A key issue for PJMIF is the required/achievable symmetry of the imploding plasma liner; this is being addressed in ongoing research [1]. Prior numerical studies [17,21] employed 3D simulations to elucidate the origin and evolution of non-uniformities seeded by shocks that form between discrete merging jets. Results based on 3D smooth-particle hydrodynamic (SPH) simulations by Cassibry et al. [17] indicated that late-time uniformity of a plasma liner formed with discrete jets was similar to that of an initially spherically symmetric liner, which is a favorable result. However, further simulations are needed to explore the effects of spatial resolution (i.e., number of particles in the simulation) and the value of artificial viscosity on the liner symmetry and its evolution. Kim et al. [21], using a 3D hydrodynamics code, provided a physical picture of plasma-liner formation via merging plasma jets and liner-uniformity evolution. These simulations predicted that "primary" shocks would form between adjacent merging jets, and then the shocked plasmas associated with the "primary shocks" would merge to form "secondary shocks." This physical picture has been verified in experiments [1]. However, in these parameter regimes, shock strength is over-predicted in single-fluid hydrodynamics codes. Further benchmarking studies, along with new 3D simulations of plasma-liner formation via the merging of up to hundreds of plasma jets, will be reported elsewhere. Indeed, a key objective of ongoing research [1] is to work toward setting requirements on and identifying limits of achievable liner uniformity.

Another key issue for PJMIF is the need to develop compatible targets that take advantage of the high implosion speed (> 50 km/s) of a spherically imploding plasma liner. Some discussions of PJMIF-relevant target formation have appeared elsewhere [24,10,25], but much further research on PJMIF-compatible target development is needed. As described by D. Ryutov [24], an interesting target for compression is a high-β (i.e., $\beta \gg 1$) object with a "tangled field" that, simultaneously, allows for reduced cross-field thermal transport (i.e., Hall parameter $\omega\tau \sim 3$) and adequate parallel electron thermal confinement time (due to the long connection length of the tangled field). Because $\beta \sim 10$, it is expected that the issue of magnetohydrodynamic (MHD) instability would be sidestepped entirely because there is not enough free energy in the magnetic field to instigate virulent global instabilities. D. Ryutov [24] lays out detailed requirements for such a target to satisfy the above properties but recognizes that creation of such a target plasma "may not be a simple task." He also states that "an intuitively appealing way for creating such a target would be the use of numerous plasma guns generating small-scale, magnetized plasma bunches and injection of such bunches into a limited volume." This is precisely the plan which we intend to pursue in the near future. The high implosion speed (> 50 km/s) of a spherically imploding plasma liner, enabling the compression of a several-cm-radius plasma target in ~ 1 μs, is what enables the possibility of near-adiabatic heating of such a novel, high-β plasma target.

The remainder of the paper is organized as follows. Section 2 presents PJMIF reactor-relevant plasma-liner parameters in order to identify the relevant physics criteria for a subscale experiment. Section 3 concisely states these criteria. Section 4 uses the criteria to derive the minimum liner kinetic energy and mass for a relevant subscale experiment. Finally, Sec. 5 summarizes the main results of the paper.

2 PJMIF reactor-relevant plasma-liner parameters

We start by considering the PJMIF reactor-relevant parameter regime. Table 1 summarizes the desired physical parameters of the target at stagnation and the imploding spherical plasma liner at the time of peak ρv^2. The peak target thermal pressure p at stagnation is limited by the peak liner ρv^2. One-dimensional radiation-hydrodynamic simulations aimed at reaching the conditions in Table 1 have shown fusion energy gains up to 30 [11], where the gain is defined as the fusion energy divided by the initial liner kinetic energy. Similar cases were studied further using a 1D semi-analytic model of PJMIF [23]. These promising configurations were origi-

nally identified through hundreds of 1D simulations by one of the authors.

The required plasma-liner conditions at the time of peak ρv^2 dictate the plasma-jet initial conditions as well as the range of plasma-liner parameters over the entire implosion from the jet-merging radius r_m down to the stagnation radius $r_{\rm stag}$, which are connected through the following relations,

$$\rho_0 \sim \rho_{\rm stag} \left(\frac{r_{\rm stag}}{r_m} \right)^2 \qquad (1)$$

and

$$M_{\rm liner} = \frac{2E_0}{v^2} \approx 4\pi r_m^2 L \rho_0, \qquad (2)$$

where $\rho_0 = n_0 m$ and n_0 are the liner mass density and ion number density at r_m, respectively, $\rho_{\rm stag}$ the liner mass density just prior to reaching $r_{\rm stag}$, $M_{\rm liner}$ the total liner mass, E_0 the liner kinetic energy at r_m, v the liner implosion speed (assumed to be constant from r_m to just before $r_{\rm stag}$), L the liner thickness at r_m, and m the atomic mass of the liner species. Note that Eq. (1) holds strictly only for a 1D steady-state convergent flow with constant v and constant polytropic index γ. In a real plasma-liner system, these assumptions are not expected to hold exactly; nevertheless, Eq. (1) provides an adequate method for our present need to obtain an approximate relationship between ρ_0 and $\rho_{\rm stag}$.

Using $\rho_{\rm stag} = 3.06$ g/cm^3 and $r_{\rm stag} = 0.4$ cm from Table 1, then Eq. (1) gives $\rho_0 r_m^2 = 0.50$ g/cm. Using the latter and setting $E_0 = 25$ MJ, then $M_{\rm liner} = 1.02 \times 10^{-2}$ kg and $L = 1.62$ cm. Equation (2) shows that L is fixed once $\rho_{\rm stag} r_{\rm stag}^2 (= \rho_0 r_m^2)$, E_0, and v are fixed. Figure 1 plots r_m versus n_0 for Xe, Kr, Ar, and Ne (ion-to-proton mass ratios $\mu = 131.29, 83.80, 39.95,$ and 20.17, respectively), showing that we are limited to Xe and Kr liners if we restrict ourselves to $r_m \lesssim 2$ m and $n_0 \lesssim 10^{17}$ cm^{-3}.

We proceed with estimating the important plasma, equation-of-state (EOS), and hydrodynamic quantities of this reference PJMIF scenario. We focus on the use of xenon in assessing the PJMIF reactor-relevant regime because xenon gives the highest ρ_0 for a given n_0 and the highest Mach number $M \equiv v/C_s$ (where $C_s \equiv [\gamma k (Z T_e + T_i)/m]^{1/2}$ is the ion sound speed) for given T and v.

2.1 Liner plasma-physics properties

2.1.1 Collisionality

The thermal ion and electron collision times, τ_i and τ_e, respectively, in the plasma liner, for a range of relevant T $(= T_i = T_e$ assumed) and ion density n_i from r_m
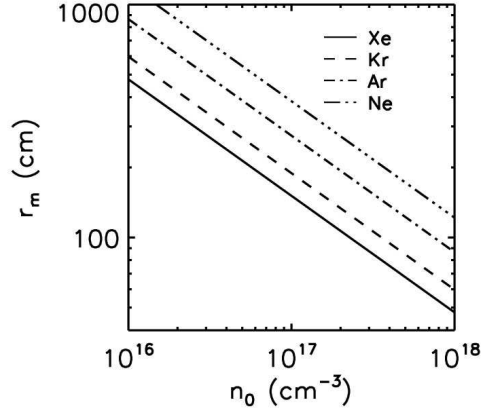

Fig. 1 Liner merging radius r_m vs. liner ion density n_0 at r_m, satisfying $\rho_0 r_m^2 = 0.50$ g/cm, for Xe, Kr, Ar, and Ne.

down to $r_{\rm stag}$, are shown in Fig. 2 for xenon. The jogs in the $\tau_i \sim Z^{-4} n_i^{-1} T^{3/2}$ contours are due to a transition from $Z = 1$ ($\tau_i \sim n_i^{-1} T^{3/2}$) to $Z \approx 0.63 T^{1/2}$ ($\tau_i \sim n_i^{-1} T^{-1/2}$) when T exceeds 2.5 eV (up to a temperature at which xenon becomes fully stripped). The $Z \sim T^{1/2}$ relation is a convenient way to model increasing Z with rising T [26]. In contrast, $\tau_e \sim Z^{-1} n_i^{-1} T^{3/2} \sim n_i^{-1} T$ exhibits a milder jog at the same transition. Figure 2 shows that the plasma liner is very collisional from r_m down to $r_{\rm stag}$, with $\tau_i < 50$ ns and $\tau_e < 0.1$ ns for the entire evolution (assuming that n_i remains above 10^{16} cm^{-3} and T remains below 10 eV). The ion–electron energy equilibration time is $\tau_{Eie} \sim (m_i/m_e)\tau_e$. For most of the liner evolution, $\tau_{Eie} \ll \tau_{\rm implosion} \approx r_m/v \approx 21.4$ μs (for $r_m = 150$ cm and $v = 70$ km/s), meaning that $T_e \approx T_i$ is a good approximation. The only exception is right at jet merging when the ions are shock heated over a microsecond time scale when the liner is at relatively low density, in which case $\tau_{Eie} \sim 2.4$ μs for $n \sim 10^{17}$ cm^{-3} and $T \approx 5$–10 eV. However, $T_e \approx T_i$ should likely be restored long before stagnation. The degree of separation between T_i and T_e due to ion shock heating is the focus of ongoing research [1] and will be reported further elsewhere. The key conclusion here is that a reactor-relevant plasma liner is highly collisional for its entire evolution.

2.2 Liner equation-of-state and radiative properties

Non-local-thermodynamic-equilibrium (non-LTE) EOS and opacity tables are used to infer the EOS (Figs. 3–4), opacity [Fig. 5(a)], and radiative-cooling [Fig. 5(b)] properties of a reactor-relevant xenon plasma liner for parameters spanning r_m to $r_{\rm stag}$. The tables were generated using PROPACEOS [27], an EOS and opacity code with detailed configuration accounting. Of partic-

Table 1 Summary of reference PJMIF target parameters at peak compression and liner parameters at the time of peak ρv^2 just prior to peak compression. The M estimate assumes $T_e = T_i = 2$ eV, $Z = 1$, and $\gamma = 1.3$.

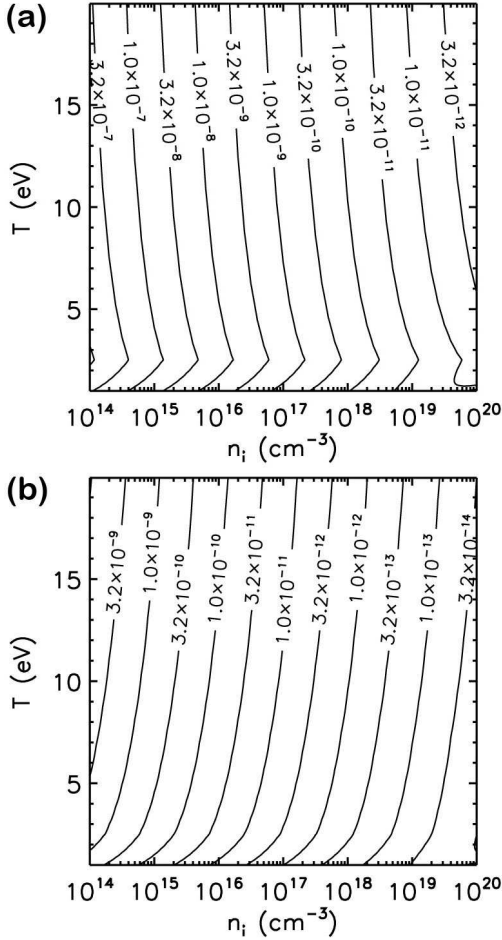| parameter	target (DT)	liner (Xe)	liner (Kr)	liner (Ar)
pressure (Mbar)	$p = 150$	$\rho v^2 = 150$	$\rho v^2 = 150$	$\rho v^2 = 150$
mass density ρ (g/cm^3)	0.02	3.06	3.06	3.06
ion density n_i (cm^{-3})	5×10^{21}	1.40×10^{22}	2.19×10^{22}	4.59×10^{22}
velocity v (km/s)	0	70	70	70
compressed target radius r_{stag} (cm)	0.4			
Mach number M		36	29	20

Fig. 2 Contours of thermal (a) ion τ_i and (b) electron τ_e collision times (s) vs. T ($= T_i = T_e$) and n_i for xenon. A simple model for ionization, $Z = 0.63 T^{1/2}$, is used [26].

ular interest is the value of γ in the xenon liner over the range of plasma-liner parameters spanning r_m to r_{stag}. Using the non-LTE EOS table, we evaluate γ for xenon using the relationship [28]

$$\gamma = \frac{p}{\rho\epsilon} + 1, \qquad (3)$$

where ϵ is the total internal energy including both thermal and ionization/excitation energies, and show the results in Fig. 6. Equation (3) shows that a larger ϵ for

given p and ρ will bring γ closer to unity (i.e., below $\gamma = 5/3$ of an ideal gas); a decrease of γ below $5/3$ is a measure of the extra energy sinks due to ionization and atomic excitation (and associated line radiation) over that of an ideal gas. Figure 6 shows that for the entire range of T (assuming $T_e = T_i$) and n_i, and in particular for the most-relevant range of $T \sim 0.1$–10 eV during plasma-liner convergence, $\gamma \lesssim 1.25$. This is desirable in order to keep the plasma liner cold and to maintain a high M during convergence, as discussed in Sec. 2.3.1. The same EOS/opacity tables are also used as input to 1D radiation-hydrodynamic simulations of spherically imploding plasma liners, which are described in Sec. 2.3.2. Although the opacity [Fig. 5(a)] and radiative-cooling [Fig. 5(b)] data are not used explicitly in the analyses in this paper, they are used in the simulation of a plasma-liner implosion in Sec. 2.3.2 and are included here for reference.

2.3 Hydrodynamic properties

2.3.1 Mach number

Because the peak liner ram pressure is expected to scale as $M^{3/2}$ [15,16], it is desirable to achieve high M, which will also reduce the amount of jet spreading and density degradation as the jets propagate from the guns to r_m [23]. Achieving $M \geq 10$ in a subscale experiment is a reasonable criterion to be in a physics regime that is relevant to a reactor-relevant plasma liner. Figure 7 shows M (as defined in Sec. 2) versus liner implosion speed for different species. For helium, $v \gtrsim 100$ km/s is needed for $M = 10$, but for nitrogen (and heavier elements), $v \gtrsim 50$ km/s (or lower for heavier elements) is sufficient.

2.3.2 Simulation

To develop knowledge of the plasma-liner parameters from r_m to r_{stag}, we used HELIOS [27], a 1D radiation-hydrodynamic code, to simulate an imploding 1.62-cm-thick xenon plasma liner, starting at $r_m = 150$ cm with
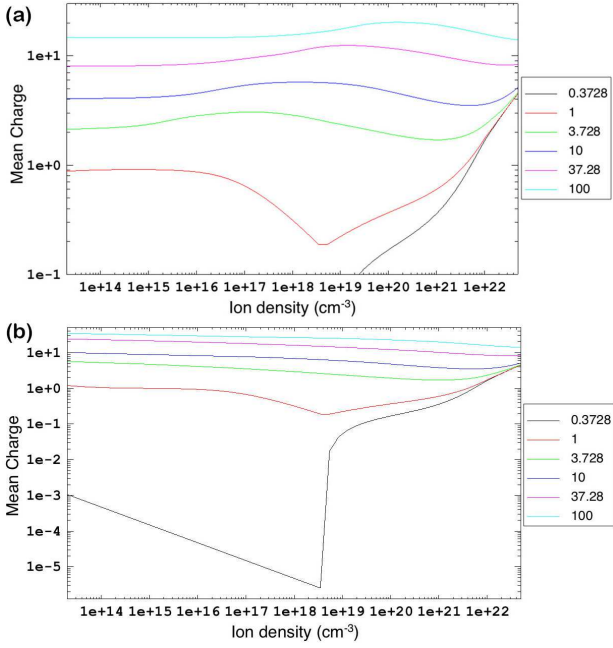
Fig. 3 Mean-charge state Z of xenon vs. ion density for different temperatures (in eV), from (a) non-LTE and (b) LTE PROPACEOS calculations. Differences between the two models are pronounced at lower densities, indicating that a non-LTE model should be used for the early stages of liner convergence.
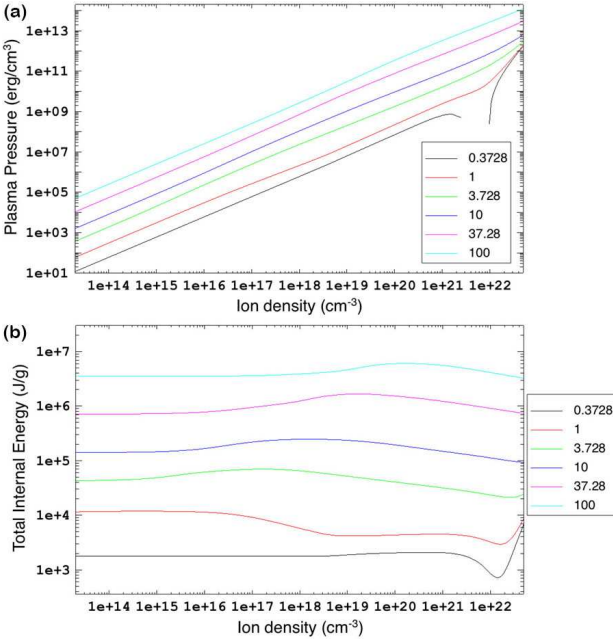

Fig. 4 (a) Total thermal plasma pressure and (b) internal energy (including ion and electron thermal and ionization/excitation energies) of xenon vs. ion density for different temperatures (in eV), from a non-LTE PROPACEOS calculation.
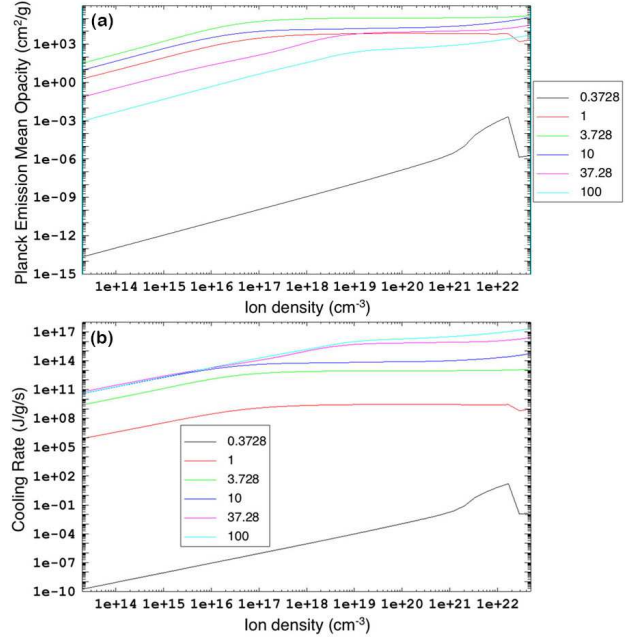

Fig. 5 (a) Frequency-integrated Planck emission mean opacity and (b) radiative-cooling rate of xenon vs. ion density for different temperatures (in eV), from a non-LTE PROPACEOS calculation.
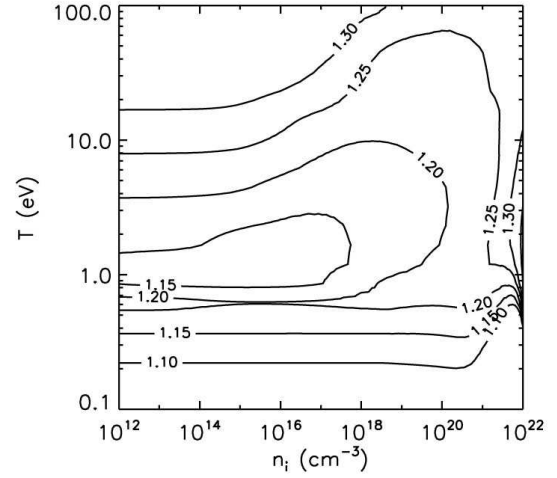

Fig. 6 Contours of polytropic index γ as a function of T $(= T_e = T_i)$ and n_i, calculated using Eq. (3) and a non-LTE xenon EOS from PROPACEOS.

spatially uniform $v = 70$ km/s, $n_0 = 10^{17}$ cm^{-3}, and $T_e = T_i = 2$ eV. Note that this simulation does not include a magnetized target; it is a xenon liner imploding on vacuum. The simulation uses non-LTE xenon EOS/opacity data [Figs. 3(a), 4, and 5] generated using PROPACEOS, includes thermal and radiation transport, and allows T_e and T_i to evolve separately. The liner is modeled using 300 computational zones (i.e., an average of 54 μm/zone at the initial time step). Figure 8 shows the temporal and spatial evolution of ρ and ρv^2, the peak values of which are 0.72 g/cc and 26.7 Mbar,
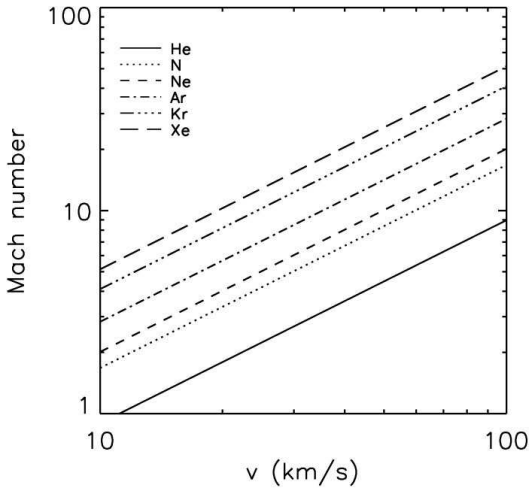
Fig. 7 Mach number M versus liner implosion speed for different liner species, assuming $T_e = T_i = 2$ eV, $Z = 1$, and $\gamma = 1.3$.

respectively, at $t = 21.6$ μs and $r = 1.16$ cm. Optimization of liner parameters and profiles, e.g., see [29], is needed in order to achieve the desired peak ram pressure of 150 Mbar at the same initial kinetic energy.

3 Physics criteria to be satisfied in a subscale plasma liner experiment

The results in Sec. 2 guide us to the important physics criteria that must be satisfied in a subscale plasma liner experiment to be of relevance to the full-scale reactor-relevant plasma liner. We state them as follows:

- $M > 10$ at r_m
- plasma must be collisional for the entire duration from r_m to $r_{\rm stag}$, i.e., $\tau_i \ll \tau_{\rm implosion}$
- effective γ of the liner species should be $< 5/3$ as is the case for xenon.

4 Requirements for a subscale plasma liner experiment

We use Eq. (2) to estimate M and E_0 of a subscale plasma liner experiment that satisfies the physics criteria stated in Sec. 3. Rather than fixing $\rho_{\rm stag} r_{\rm stag}^2$ as we did for the PJMIF-reactor scenario, we use the criteria stated in Sec. 3 and the constraints of the PLX vacuum chamber and near-term plasma guns to set r_m, L, n_0, v, and m, picking the lowest allowed values for each quantity in order to minimize E_0 and $M_{\rm liner}$ of a subscale experiment.
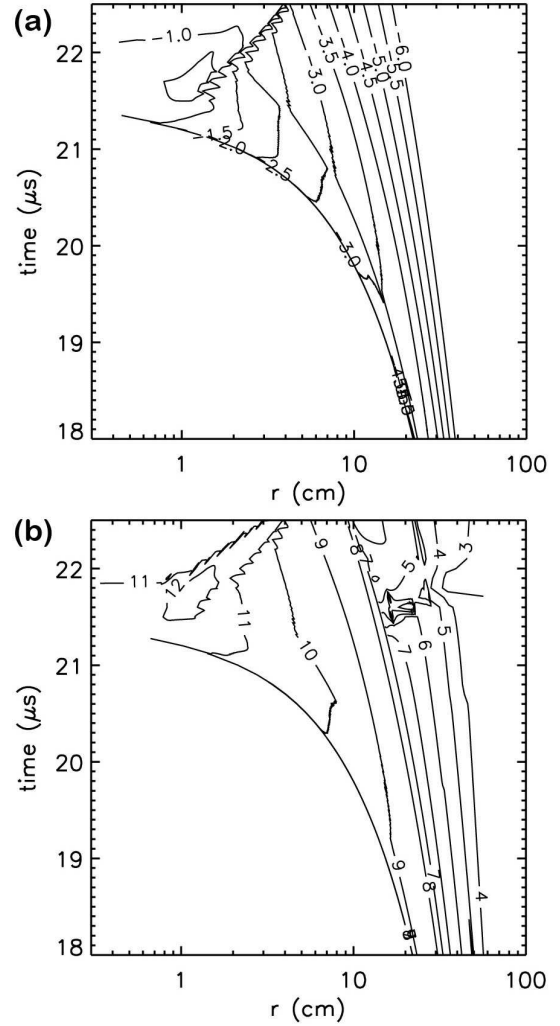

Fig. 8 Contours of constant (a) $\log(\rho$ [g/cc]) and (b) $\log(\rho v^2$[Pa]) vs. time and radius for a PJMIF reactor-relevant, imploding xenon plasma liner, from a HELIOS simulation. Peak $\rho = 0.72$ g/cc and $\rho v^2 = 26.7$ Mbar are reached at $t = 21.6$ μs and $r = 1.16$ cm.

First, we determine r_m, which is given by (and plotted in Fig. 9) [20]

$$r_m = \frac{r_{j0}[M_j(\gamma - 1)/2 + 1] + r_w}{1 + (2/N^{1/2})[M_j(\gamma - 1)/2 + 1]},\qquad(4)$$

where r_{j0} is the initial jet radius, M_j the initial jet Mach number, r_w the chamber-wall radius (where jets are launched), and N the number of jets. Equation (4) includes the effect of jet spreading at the maximum rate $2C_s/(\gamma - 1)$, where C_s is the sound speed, and thus provides an upper bound on r_m. We choose $r_m = 75$ cm as an upper bound, corresponding to $N = 60$ and $M = 10$ (see Fig. 9). Lower N and higher M will result in lower r_m and therefore lower E_0.

To determine L, we assume that the initial jet length equals L at r_m. Upgrades to pulsed coaxial guns [30] for the subscale plasma-liner-formation experiments were
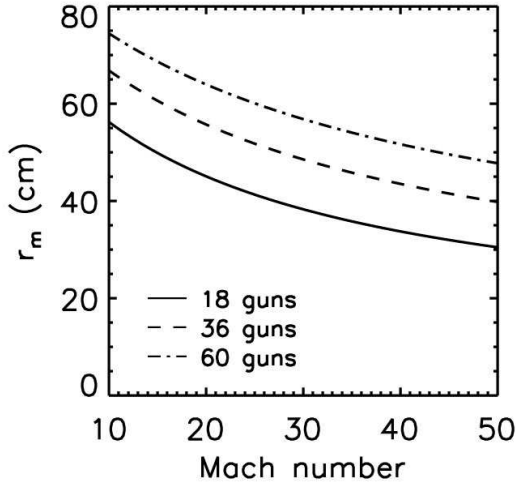
Fig. 9 Jet-merging radius r_m vs. M for different numbers of plasma jets, assuming $r_{j0} = 5$ cm, $r_w = 110$ cm, and $\gamma = 1.3$.

expected to achieve $L = 10$ cm (and indeed recently have done so [31]), and thus we use $L = 10$ cm.

The minimum n_0 at r_m is determined based on satisfying the collisionality requirement $\tau_i \ll \tau_{\mathrm{implosion}}$, i.e.,

$$\frac{\tau_i}{\tau_{\mathrm{implosion}}} = \frac{(4.80 \times 10^{-8} Z^4 \mu^{-1/2} n_i \log \Lambda T_i^{-3/2})^{-1}}{r_m/v} \ll 1$$

$$\rightarrow n_i \gg \frac{\mu^{1/2} T_i^{3/2} v}{4.80 \times 10^{-8} Z^4 \log \Lambda r_m} \approx 2 \times 10^{12} \text{ cm}^{-3},$$

where we have used $\mu = 14.01$ (nitrogen), $T = 2$ eV, $v = 50$ km/s, $Z = 1$, $\log \Lambda = 7$, and $r_m = 75$ cm. Thus, we set $n_0 > 10^{14}$ to strongly satisfy the collisionality requirement. Note that if T rises during liner convergence, the minimum n_0 requirement will decrease due to the $T_i^{3/2}/Z^4 \sim T_i^{-1/2}$ scaling (where, again, $Z \sim T^{1/2}$ is used as a simple model for ionization).

For v, we refer to Fig. 7 to see that we must have $v \approx 50$ km/s to have $M \approx 10$ for nitrogen, which is the lowest-mass element being considered that will allow us to get $M = 10$ while staying well below $v = 100$ km/s.

Finally, using Eq. (3) and a PROPACEOS non-LTE nitrogen EOS, we verify that $\gamma < 5/3$ for a nitrogen plasma liner so as to have the desirable energy sink from ionization and atomic excitation to keep M high, as exhibited by xenon (Fig. 6). Figure 10(a) shows that a nitrogen plasma liner in a subscale experiment would have $\gamma < 1.3$ for the most-relevant range of $T \sim 1$–10 eV. Argon, which is also being used extensively in the subscale experiment, has $\gamma < 1.4$ for the same range [Fig. 10(b)].

With the values $r_m = 75$ cm, $L = 10$ cm, $n_0 = 10^{14}$ cm^{-3}, $v = 50$ km/s, and nitrogen as the liner species, Eq. (2) tells us that $E_0 = 2.1$ kJ and $M_{\mathrm{liner}} = 1.65$ mg. To obtain scaling data in the subscale experiment with species up to xenon would require nearly a
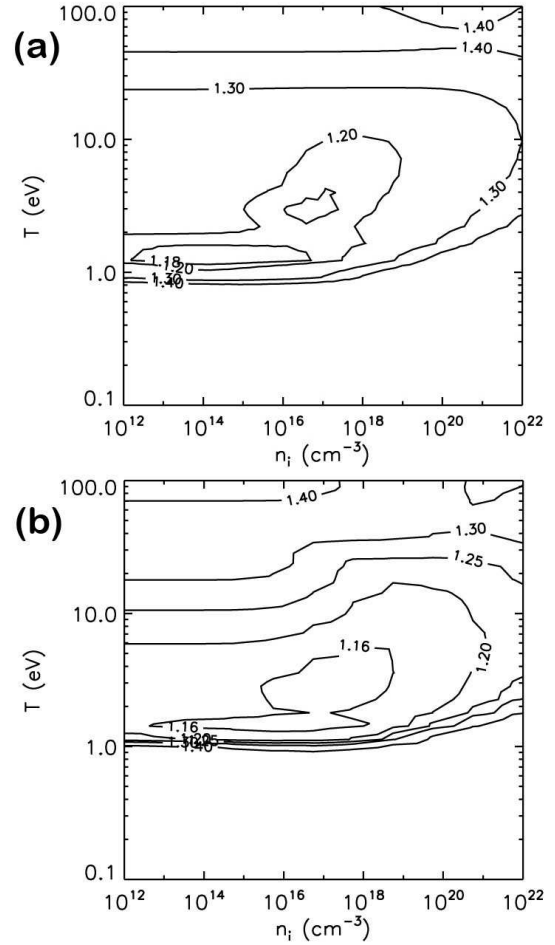

Fig. 10 Contours of polytropic index γ as a function of T ($= T_e = T_i$) and n_i for (a) nitrogen and (b) argon, calculated using Eq. (3) and non-LTE EOS tables from PROPACEOS.

factor of ten higher mass (15.4 mg) and energy (19.7 kJ). To further scale up n_0 an order of magnitude or v up by a factor of three (or some combination thereof) would require another factor of ten higher in energy, resulting in $E_0 \approx 200$ kJ for the ideal subscale plasma-liner-formation experiment, capable of a decade in energy scaling for the heaviest element xenon.

Due to budgetary constraints, the subscale plasma-liner-formation experiment now being developed [1] is expected to culminate with $N = 36$ guns and total capacitor stored energy of $E_{\mathrm{cap}} = 260$ kJ. For $M = 10$ and $N = 36$, Fig. 9 shows that $r_m \approx 65$ cm. Using $v = 50$ km/s and $L = 10$ cm, Eq. (2) gives $E_0 = 14.5$ kJ for xenon. If the gun electrical efficiency is $\eta = 0.25$ (as suggested by the ongoing work [31,1]), then the maximum liner energy is $\eta E_{\mathrm{cap}} = 65$ kJ, meaning there is still a reasonable factor of 4.5 headroom above $E_0 = 14.5$ kJ (xenon) for scaling studies. Lower-mass species would have a higher headroom in energy for scaling studies.

5 Summary

We laid out the key requirements of a subscale plasma-liner-formation experiment to produce data of direct relevance for addressing key scientific issues of a full-scale, reactor-relevant plasma liner. The key scientific issues of plasma-liner formation via merging hypersonic plasma jets being addressed in the near term are: (1) determining the scaling of peak liner ram pressure with initial plasma-jet parameters, and (2) assessing liner non-uniformity and prospects for non-uniformity control.

To ensure that a subscale plasma-liner-formation experiment can address the above issues in a way that is relevant to the full-scale plasma liner, we identified key physics criteria that must be satisfied in the subscale experiment. These criteria are: (1) the plasma liner must be very collisional all the way from the merging radius to stagnation, (2) the liner Mach number must be high, i.e., $M > 10$, (3) the liner species must satisfy $M > 10$ while possessing the EOS and radiative properties, i.e., $\gamma < 5/3$, of a high-Z species such as Xe, as desired in a fusion-relevant liner.

A thirty-six-gun experiment with liner kinetic energy up to $E_0 = 65$ kJ that satisfies the physics criteria and requirements presented in this paper is now under development [1].

References

1. S.C. Hsu, S.J. Langendorf, K.C. Yates, J.P. Dunn, S. Brockington, A. Case, E. Cruz, F.D. Witherspoon, M.A. Gilmore, J.T. Cassibry, R. Samulyak, P. Stoltz, K. Schillo, W. Shih, K. Beckwith, Y.C.F. Thio, IEEE Trans. Plasma Sci. **PP**(99), 1 (2017). DOI 10.1109/TPS.2017.2779421
2. S.C. Hsu, E.C. Merritt, A.L. Moser, T.J. Awe, S.J.E. Brockington, J.S. Davis, C.S. Adams, A. Case, J.T. Cassibry, J.P. Dunn, M.A. Gilmore, A.G. Lynn, S.J. Messer, F.D. Witherspoon, Phys. Plasmas **19**, 123514 (2012)
3. S.C. Hsu, A.L. Moser, E.C. Merritt, C.S. Adams, J.P. Dunn, S. Brockington, A. Case, M. Gilmore, A.G. Lynn, S.J. Messer, F.D. Witherspoon, J. Plasma Phys. **81**, 345810201 (2015)
4. J.J. Bertin, R.M. Cummings, *Aerodynamics for Engineers, Sixth Edition* (Pearson, Upper Saddle River, NJ, 2013)
5. I.R. Lindemuth, R.C. Kirkpatrick, Nucl. Fusion **23**, 263 (1983)
6. R.C. Kirkpatrick, I.R. Lindemuth, M.S. Ward, Fusion Tech. **27**, 201 (1995)
7. I.R. Lindemuth, R.E. Siemon, Amer. J. Phys. **77**, 407 (2009)
8. Y.C.F. Thio, E. Panarella, R.C. Kirkpatrick, C.E. Knapp, F. Wysocki, P. Parks, G. Schmidt, in *Current Trends in International Fusion Research–Proceedings of the Second International Symposium*, ed. by E. Panarella (NRC Canada, Ottawa, 1999), p. 113
9. Y.C.F. Thio, C.E. Knapp, R.C. Kirkpatrick, R.E. Siemon, P.J. Turchi, J. Fusion Energy **20**, 1 (2001)
10. S.C. Hsu, T.J. Awe, S. Brockington, A. Case, J.T. Cassibry, G. Kagan, S.J. Messer, M. Stanic, X. Tang, D.R. Welch, F.D. Witherspoon, IEEE Trans. Plasma Sci. **40**, 1287 (2012)
11. C.E. Knapp, R.C. Kirkpatrick, Phys. Plasmas **21**, 070701 (2014)
12. "Conceptual Cost Study for a Fusion Power Plant Based on Four Technologies from the DOE ARPA-E ALPHA Program," Bechtel National, Inc., Report No. 26029-000-30R-G01G-00001 (2017).
13. P.B. Parks, Phys. Plasmas **15**, 062506 (2008)
14. R. Samulyak, P. Parks, L. Wu, Phys. Plasmas **17**, 092702 (2010)
15. T.J. Awe, C.S. Adams, J.S. Davis, D.S. Hanna, S.C. Hsu, J.T. Cassibry, Phys. Plasmas **18**, 072705 (2011)
16. J.S. Davis, S.C. Hsu, I.E. Golovkin, J.J. MacFarlane, J.T. Cassibry, Phys. Plasmas **19**, 102701 (2012)
17. J.T. Cassibry, M. Stanic, S.C. Hsu, F.D. Witherspoon, S.I. Abarzhi, Phys. Plasmas **19**, 052702 (2012)
18. H. Kim, R. Samulyak, L. Zhang, P. Parks, Phys. Plasmas **19**, 082711 (2012)
19. E.C. Merritt, A.L. Moser, S.C. Hsu, J. Loverich, M. Gilmore, Phys. Rev. Lett. **111**, 085003 (2013)
20. J.T. Cassibry, M. Stanic, S.C. Hsu, Phys. Plasmas **20**, 032706 (2013)
21. H. Kim, L. Zhang, R. Samulyak, P. Parks, Phys. Plasmas **20**, 022704 (2013)
22. E.C. Merritt, A.L. Moser, S.C. Hsu, C.S. Adams, J.P. Dunn, A. Miguel Holgado, M.A. Gilmore, Phys. Plasmas **21**, 055703 (2014)
23. S.J. Langendorf, S.C. Hsu, Phys. Plasmas **24**, 032704 (2017)
24. D.D. Ryutov, Fus. Sci. Tech. **56**, 1489 (2009)
25. D.R. Welch, T.C. Genoni, C. Thoma, D.V. Rose, S.C. Hsu, Phys. Plasmas **21**, 032704 (2014)
26. R.P. Drake, *High-Energy-Density-Physics* (Springer-Verlag, Berlin, 2010)
27. J.J. MacFarlane, I.E. Golovkin, P.R. Woodruff, J. Quant. Spect. Rad. Transfer **99**, 381 (2006)
28. Y.A. Zel'dovich, Y.P. Raizer, *Physics of Shock Waves and High-Temperature Hydrodynamic Phenomena* (Academic Press, New York, 1966)
29. G. Kagan, X. Tang, S.C. Hsu, T.J. Awe, Phys. Plasmas **18**, 120702 (2011)
30. F.D. Witherspoon, A. Case, S.J. Messer, R. Bomgardner II, M.W. Phillips, S. Brockington, R. Elton, Rev. Sci. Instrum. **80**, 083506 (2009)
31. A. Case, S. Brockington, E. Cruz, F.D. Witherspoon, Bull. Amer. Phys. Soc. **62**, 395 (2017)